Scientia Iranica (2024) 31(12), 920–934

SCIENTIA
IRANICA

Sharif University of Technology
Scientia Iranica
Transactions F: Nanotechnology
https://scientiairanica.sharif.edu

Tuning the preferential direction of ion flow in asymmetric nanofluidic mediums

M. Bakirci[a,*] **and R. Garren**[b]

a. *Faculty of Aeronautics and Astronautics, Tarsus University, Mersin, 33400 Turkey.*
b. *Batten College of Engineering and Technology, Old Dominion University, Norfolk, 23529 VA.*

Received 5 December 2021; received in revised form 31 October 2022; accepted 18 April 2023

KEYWORDS
Electrokinetic flow;
Thermoplastic polyurethane;
Current rectification;
Nanochannel;
Continuum model.

Abstract. Current rectification and electrokinetic flow properties in an asymmetric nanochannel in a thermoplastic polyurethane membrane were investigated experimentally and numerically. The nanochannel with a tip diameter of about 300 nm showed current rectification, which is evident only in nanochannels with much smaller tip radii (<100 nm), due to the surface properties of the thermoplastic polyurethane material. To elucidate the mechanism of current rectification, a mathematical model consisting of Nernst-Planck equations for the ionic mass transport, the Poisson's equation for electrostatics, and Navier-Stokes equations for flow field has been developed. It was verified that the obtained numerical results were in qualitative agreement with the experimental results obtained. It was concluded that due to the surface charge of the channel material, a significantly thick electric double layer was formed on the inner surface of the nanochannel in contact with the electrolyte, and this formed a gating mechanism because of overlapping electric double layers near the tip of the asymmetric nanochannel. It has been found that the applied concentration gradient is as effective as low applied potentials and thus can reverse the preferential direction of ion flow.

1. Introduction

Within the last two decades, nanochannels have drawn continuous attention from researchers in different disciplines. In fact the efforts in the field of nanochannels have seen significant growth mostly because of scientific and technological advancement as well as progression of nanofabrication technology. Nanochannels have found many applications in various research branches such as development of biosensors and bioelectronic devices [1–3], separation [4–6], extra small volume chemical delivery [7–9], maturation of scanning probe microscopy [9–11], and DNA sequencing [12–16]. Studies on the ion transport in channels with nano-scale sized have shown some fascinating characteristics due to the presence of Electric Double Layers (EDL) [17,18]. Indeed asymmetric nanochannels possessing overabundance surface charge and the diameter of the small opening comparable to the electrical double layer thickness of electrolyte show non-linear, diode-like current-voltage (I-V) responses [19]. This kind of phenomenon refers

---

[*]. *Corresponding author. Tel.: +90-324-600-0033*
E-mail addresses: muratbakirci@tarsus.edu.tr (M. Bakirci); rgarren@odu.edu (R. Garren)

To cite this article:
M. Bakirci and R. Garren "Tuning the preferential direction of ion flow in asymmetric nanofluidic mediums", *Scientia Iranica* (2024), **31**(12), pp. 920-934
DOI: 10.24200/sci.2023.59514.6284

to ionic current rectification (ICR) [2,9,20–35]. In other words, the magnitude of current through the nanochannel at negative potentials is greater or less than the current at positive potentials. ICR can be quantified by the ratio of the two countercurrents generated by potential gradients equal in magnitude with opposite senses.

Nanochannels produced for use in nanofluidics studies are obtained from a wide variety of materials, however, Polyethylene Terephthalate (PET) is preferred in the vast majority of these studies. Thermoplastic polyurethane (TPU) polymer structures can be a good alternative for nanochannels to be used in nanoflow and ion transport. TPU is a very useful polymer material with extraordinary physical properties and has a wide range of uses such as the automotive industry and medical products [36–39]. TPU structures have a quite important place in the structural reinforcement of elastomer materials. It has been demonstrated that Polyactic Acid (PLA) materials reinforced with TPU have a higher tensile strength and therefore prevent excessive elongation [40]. Polycaprolactone (PCL) structures reinforced with TPU have been shown to be a heat sensitive material that can show very interesting properties. Moreover, these structures have been shown to be shape memory polymers [41,42]. In another study, it has been shown that TPU and PLA based structures have the same shape memory [43]. On the other hand, it has been shown many times that PLA blended with TPU causes a high level of hardness [44,45]. TPU polymers are quite suitable for developing nanocomposite sensors due to their microphase separation nature [46]. TPU composite structures with multi-walled CNTs are a good example for developing gas detection systems [47]. In another study, a nanocomposite structure consisting of TPU and carbon nanotube was used for the production of a multiaxial force nanosensor. It has been reported that this fabricated structure is mechanically flexible due to TPU additive, and also has a significant electrical conductivity [48].

Several researchers have analyzed the mechanism of current rectification and proposed various theoretical models [49,50] to explain the origin of ICR. Despite all the different mechanisms proposed, the transport of ions in asymmetric nanochannels has yet to find a generally accepted explanation. The Poisson-Nernst-Planck (PNP) equations have widely been used to simulate the ICR behavior in nanochannels. Comparing experimental and numerical studies have shown that the continuum model properly describes ion transport and ICR in nanochannels with diameters greater than 0.1 Debye length [51,52].

In the present paper, the ICR phenomenon through an asymmetric nanochannel simultaneously subjected to an electric field and electrolyte concentration gradient is experimentally and numerically investigated. For the numerical study, the Finite Element Method (FEM) was used to address the problem. Using the mathematical model, the accuracy of which was tested through some benchmark problems [51,52], the ionic flow in the nanochannel was studied in detail. Moreover, the numerical results obtained were verified with experimental results. A TPU membrane containing an asymmetrical nanochannel was used in the experiments. Various concentration gradients were imposed between two openings of the nanochannel and the ionic rectifying effect was investigated by applying two different polarities of electrical field on the experimental setup.

2. Exprimental study

The SIOS-qNano nanochannel technology platform (Izon Company, www.izon.com) has been used for the experiments. Figure 1 illustrates the experimental setup consist of a fluid cell with upper and lower fluid wells separated by a TPU membrane containing an asymmetric nanochannel. The negatively charged carboxyl group of the TPU membrane causes the channel surface negatively charged. The control suite software collects and analyses current signals across the nanochannel from the electronic of the instrument. The software of the instrument allows a very detailed measurement of the ionic current values responsive to the applied bias voltage. In the experiments, the following five KCl solutions were examined; 1 mM, 5 mM, 10 mM, 50 mM, and 100 mM. Prior to each experiment, both fluid wells and nanochannel were washed with de-ionized water several times. Solutions were sonicated for approximately 10 minutes and then the fluid wells were filled using a 100 μm microsyringe. Prior to each experiment, any air bubbles inside the lower and upper fluid wells were removed.

The ionic current through the nanochannel was measured with silver/silver-chloride (Ag/AgCl) electrodes. These electrodes, which are largely non-polarized and very stable, are often preferred in experimental nanofluidics studies. The experimental setup includes two electrodes placed in both openings of the asymmetric nanochannel, one with the narrow opening (tip) and the other with the large opening (base), as seen in Figure 1. An imposed electric potential between these Ag/AgCl electrodes generates an ionic current through the nanochannel. The ions flowing through a nanochannel are primarily transported through this applied potential and diffusion. Temperature and pressure difference can also cause gradients but the majority of the experiments are performed at atmospheric pressure and room temperature. In the experiments, the ion current was recorded in the voltage range between -1 V to $+1$ V in steps of 100 mV. The

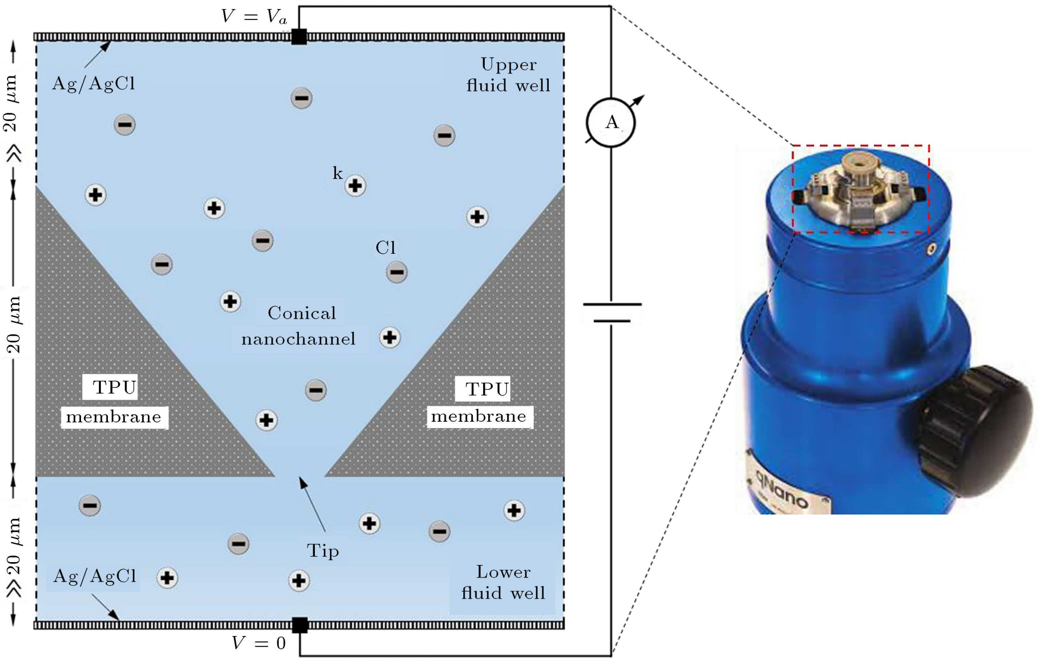

Figure 1. q-Nano device and illustration of the experimental setup.

duration at each voltage is 2.5 minutes, and each ion current recording consists of about one million data (the sampling frequency is about 6666.6 Hz). Current-voltage (I-V) curves were obtained by averaging these data of ionic current induced by the applied voltage. In the recorded data, the estimated error was about ±0.01 nA while the recorded ionic current values were from several nanoampers to 160 nA.

3. Numerical study

The mechanism of ICR and the effect of the electrolyte gradient on ICR are theoretically investigated using a continuum-based PNP-NS mathematical model, composed of the Nernst-Planck equations for the ionic mass transport, the Poisson equation for the electric potential in the electrolyte solution, and the Navier-Stokes equations for the flow field [2,27,49]. The numerical implementation and model validation were examined by several researchers [2,27] for some benchmark problems where analytical solutions exist.

While comparing the experimental and numerical results, it is necessary to note the differences between experimental setup and computational domain which may cause possible differences in results. Since the dimensions of the fluid wells are much larger than the dimensions of the nanochannel, it is almost impossible to use same scales for both. For that reason the dimensions of the computational domain must be smaller than the real setup size. Another significant difference between computational domain and experimental setup is the shape of the asymmetric nanochannel. While the nanochannel geometry is perfect in the computational domain, the actual nanochannel in the TPU membrane is not exactly perfect and its surface is not smooth, and this may cause a difference in experimental and numerical results.

Non-dimensionalization can simplify and parameterize problems where measured units are involved. It is closely related to dimensional analysis. The dimensionless form of the governing equations can be very useful for comparing the experimental and numerical results. The governing equations are transformed into non-dimensional equations by using scale parameters, so that numerical results can be qualitatively compared with the experimental results obtained.

A sketch of the computational domain and 3D CAD image for the axi-symmetric nanochannel is shown in Figure 2. As stated in the figure, the axial length of the channel, the radius of the tip and the base are respectively, L, R_t, and R_b. The identical upper and lower fluid wells filled with various electrolyte solutions to generate various concentration gradients. In order to provide the bulk ionic concentration as a constant value the dimensions of the fluid wells are selected wide enough. The wall of the nanochannel has a uniform surface charge density, which allows to form an EDL near this charged wall in the electrolyte solution. As one can assume that an applied potential between fluid wells (AB and GH) induces an ionic current through the nanochannel. In accordance with the axi-symmetric geometry of the domain, a cylindrical coordinate system has been fixed at the center of the nanochannel. In the domain, segment AH represents

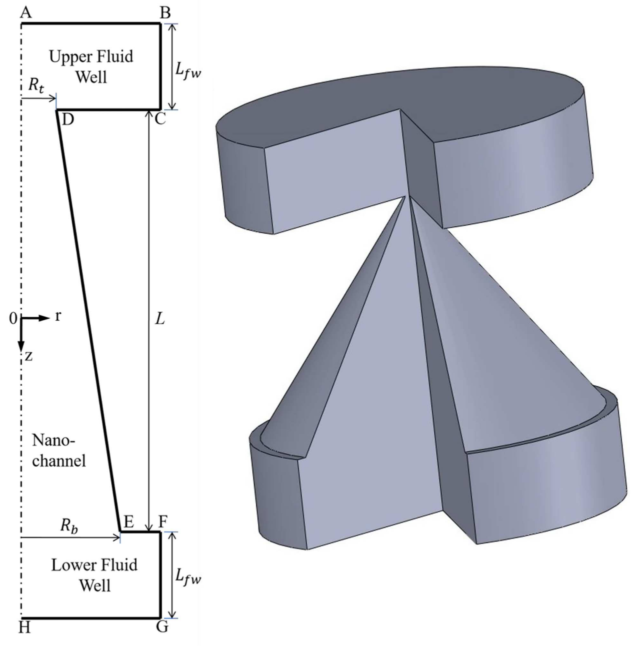

Figure 2. Sketch of the computational domain and a 3D CAD illustration.

the axis of the symmetry. Segments AB, BC, CD, EF, FG, and GH are the boundaries of the fluid wells and DE is the wall of the nanochannel.

Since the Reynolds number of the electrokinetic flow is on the scale of 10^{-6}, the inertial terms in the Navier-Stokes equations can simply be neglected. As a result an incompressible flow of an electrolyte solution is governed by:

$$\nabla \cdot u = 0, \tag{1}$$

$$-\nabla p + \mu \nabla^2 u - F\left(z_1 c_1 + z_2 c_2\right) \nabla \varphi = 0. \tag{2}$$

In these equations u denotes the fluid velocity, p is the pressure, φ is the electric potential in the electrolyte solution, c_1 and c_2 are the molar concentrations of the positive (K^+) and negative ions (Cl^-), $z_1 = +1$ and $z_2 = -1$ are the valences of the positive and negative ions respectively, and F is the Faraday constant. The interactions between applied potential and net charge in the electrolyte are taken into account by the last term of the Eq. (2). In addition to these suitable boundary conditions are properly fixed to the boundaries of the domain. Nonslip boundary conditions are set on the CD, DE, and EF segments. As mentioned before the top and bottom boundaries of the fluid wells are far away from the nanochannel therefore a normal flow with zero pressure is used for AB and GH. Since BC and FG boundaries are far away from the channel openings, slip boundary conditions are used for these segments.

A complete description of the ionic mass transport of a charged nanochannel starts with the flux equations for each aqueous species. The convection, diffusion, and migration mechanisms provide the equation for the flux density of each ionic species as stated below:

$$N_i = uc_i - D_i \nabla c_i - z_i \frac{D_i}{RT} F c_i \nabla \varphi, \tag{3}$$

where D_i is the diffusion coefficient of the ith ionic species, T is the absolute temperature of the electrolyte solution, and R is the universal gas constant. When steady state condition is assumed, Nernst-Planck equation governs the concentrations of each species as follows:

$$\nabla \cdot N_i = 0 \qquad i = 1, 2. \tag{4}$$

On the other hand the Poisson equation governs the electric potential in the electrolyte solution,

$$-\varepsilon \nabla^2 \varphi = \sum\nolimits_i z_i c_i. \tag{5}$$

Since the segment CD and EF of the fluid wells and the wall of the nanochannel (DE) are solid surfaces, it is assumed that these surfaces are impervious to ions and consequently the normal ionic flux must be zero as stated below:

$$n \cdot N_i = 0 \qquad i = 1, 2. \tag{6}$$

Here, n is the local unit normal vector of the above segments. Same boundary conditions are set for the BC and FG walls of the fluid wells which is a direct consequence of being in the bulk electrolyte wells. Similarly, since two-dimensional axisymmetric simulation is performed, zero normal ionic flux is used along AH due to the axi-symmetric condition.

As assumed the top boundary of the upper well and the bottom boundary of the lower fluid well are significantly far away from the nanochannel, therefore the ionic concentrations are considered same as the bulk concentration of the electrolyte solution.

$$c_i = C_0 \qquad i = 1, 2. \tag{7}$$

To create an electric field (potential difference) across the nanochannel, an external potential is applied along the AB edge of the upper fluid well and zero potential is applied along the GH edge of the lower fluid well respectively.

$$V = \varphi \qquad \text{and} \qquad V = 0. \tag{8}$$

The boundaries CD and EF of the fluid wells are assumed to be uncharged and because of the long distance from the nanochannel, insulation condition is set for the side boundaries BC and FG of the fluid wells as shown below:

$$n \cdot \nabla \varphi = 0. \tag{9}$$

Axi-symmetric boundary condition is used along the AH segment. Since the wall of the nanochannel is charged, the following boundary condition is set for the segment DE:

$$n \cdot (-\varepsilon \nabla \varphi) = \sigma. \tag{10}$$

Generated ionic current through the nanochannel is calculated by the integration of the current density along the surface of the anode or cathode:

$$I = \int_s F\left(z_1 N_1 + z_2 N_2\right) \cdot n ds. \tag{11}$$

In order to obtain the dimensionless form of the mathematical model, C_0 (bulk concentration), RT/F, R_t, $u_0 = \varepsilon R^2 T^2/\mu R_t F^2$, and $\mu u_0/R_t$ were used as the ionic concentration scale, potential scale, length scale, velocity scale and pressure scale respectively. Then the dimensionless governing equations become:

$$\nabla^* \cdot u^* = 0, \tag{12}$$

$$-\nabla^* p^* + \nabla^{*2} u^* - \frac{1}{2}(\kappa R_t)^2 \left(\sum_i z_i c_i^*\right) \nabla^* \varphi^* = 0, \tag{13}$$

$$\nabla^* \cdot N_i^* = 0 \qquad i = 1, 2, \tag{14}$$

$$-\nabla^{*2} \varphi^* = \frac{1}{2}(\kappa R_t)^2 \sum_i z_i c_i^*. \tag{15}$$

In these equations, the superscript $(^*)$ denotes the dimensionless variables and $\kappa^{-1} = \left(\varepsilon RT/2F^2 C_0\right)^{1/2}$ is the Debye length. The term $U_0 C_0$ is used to obtain the dimensionless form of the flux density as follows:

$$N_i^* = u^* c_i^* - \Lambda_i \nabla^* c_i^* - z_i \Lambda_i c_i^* \nabla^* \varphi^*, \tag{16}$$

where $\Lambda_i = D_i/D_0$ and $D_0 = \varepsilon R^2 T^2/\mu F^2$. The equation for the ionic current through the nanochannel is normalized with the expression of $F U_0 C_0 R_t^2$ and took the form below:

$$I^* = \int \left(z_1 N_1^* + z_2 N_2^*\right) \cdot n ds^*. \tag{17}$$

4. Results

4.1. Experimental results

Experiments were started by applying zero potential across the nanochannel and increased up to I V in 100 mV increments. After obtaining the current value for +1 V potential, the applied potential was set back to zero for five seconds and then gradually reduced to −1 V in 100 MV decreases. Thus, two electrical fields with same magnitude but opposite polarity were applied between the fluid wells. In this case, the fluid wells can be polarized, thus, the migration of ions and the possible polarization scenario must be considered. This was examined by a test, the results of which are shown in Figure 3.

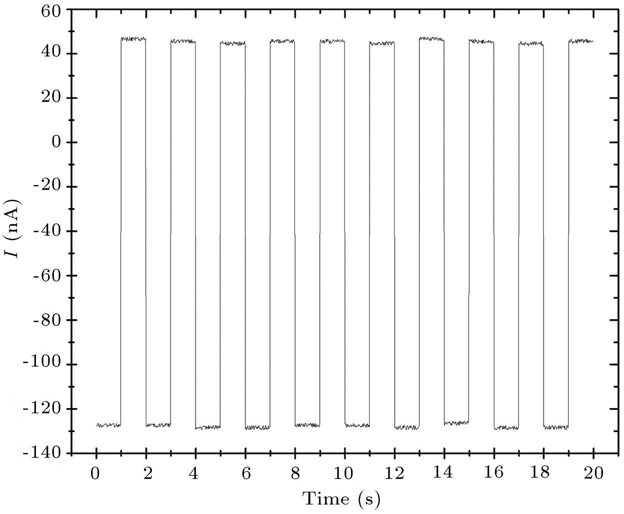

Figure 3. Reversible variation of ionic current upon switching voltage between ±1 when $C_U/C_L = 1$.

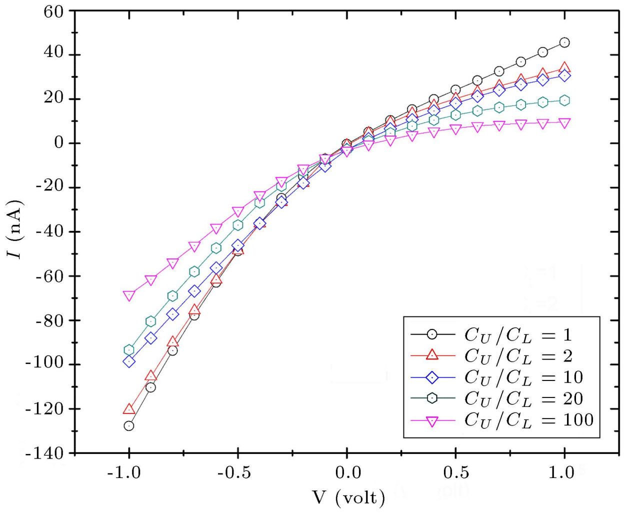

Figure 4. Ionic current variation with applied voltage across various electrolyte gradients ($C_u/C_l \geq 1$).

The reproducibility as well as reversibility of the experiments were examined by measuring the variation of the ionic current upon switching the applied voltage between +1 V and −1 V as shown in Figure 3. After the experimental setup was prepared, the direction of theapplied potential was changed every second for 20 seconds. It was observed that polarization did not occur in the fluid wells throughout the test. Thus, it was concluded that the variation of the ion current flowing through the asymmetric nanochannel is highly reversible and reproducible.

In the first set of experiments, the concentration of the upper fluid well (C_U) was fixed at 100 mM KCl while the concentration of the lower fluid well (C_L) was gradually changed. Figure 4 shows the current-voltage (I-V) characteristics of a single asymmetric nanochannel for different electrolyte concentration gradients. The case in which both the upper and lower fluid wells are fixed with 100 Mm KCl, that is, there is no concentration gradient, was called the *reference case*. The magnitude of the current corresponding to the −1 V potential is approximately 3 times the current

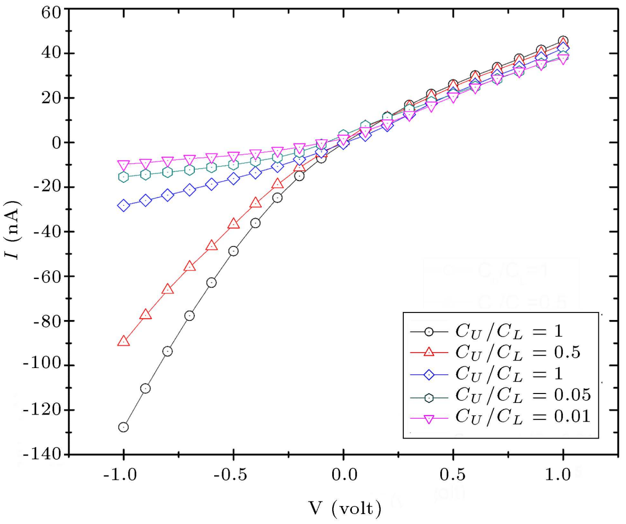

Figure 5. Ionic current variation with applied voltage across various electrolyte gradients ($C_u/C_l \leq 1$).

corresponding to the +1 V potential and therefore the current rectification is clearly visible in the reference case. As can be seen from the figure, the applied concentration gradient also affects the current-voltage (I-V) curve. In the experiment, the positive ionic current is defined as a current directed from the large opening (base) toward the small opening (tip) when a positive voltage ($V = \varphi_{base} - \varphi_{tip} > 0$) is applied. Figure 4 also reveals that the magnitude of the negative ionic current under a negative voltage is higher than the corresponding ionic current for an applied positive voltage, consistent with the existing experimental and numerical studies [2,23,25,27,28,43]. As a result, there is a preferential direction for ionic current flow and this direction is from the tip toward the base. This fact can be seen in the reference case as well. When there was no concentration gradient, the magnitude of the negative ionic current was much higher than the positive ionic current.

In the second set of experiments, the concentration of the lower fluid well was fixed at 100 mM KCl while the concentration of the upper fluid well was gradually changed and the results are presented in Figure 5. When the concentration in the upper fluid well is above a critical value, the magnitude of the negative current is greater than when the polarity of the voltage is reversed. However, when the concentration in the upper fluid well is below the critical value, the direction of the ICR is reversed, and the magnitude of the current for a positive voltage is higher than for a negative voltage of the same magnitude. Therefore, the degree and direction of the ICR can be controlled by adjusting the electrolyte concentrations in the two fluid wells. The degree of ICR is characterized by the current Rectification Ratio (RR), defined as, $RR = |(I_{-V_i}) / (I_{+V_i})|$. $RR > 1$ indicates that the magnitude of the resulting ionic current for $V < 0$ is greater than when the polarity of the applied bias voltage is reversed and vice versa.

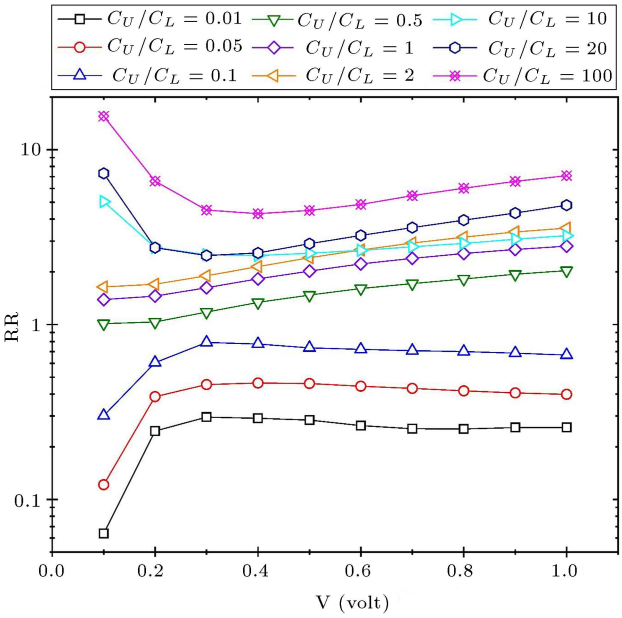

Figure 6. Current rectification ratio as a function of the applied potential difference across the nanochannel cosrresponding to Figures 4 and 5.

Figure 6 depicts the current RR as a function of the magnitude of the applied bias voltage under the same conditions as Figures 4 and 5. In the case of $C_U/C_L = 100$ where the concentration ratio is the highest, the highest RR values are obtained for all applied potential values. Conversely, in the case of $C_U/C_L = 1$ where the concentration ratio is the lowest, the lowest RR values are obtained for all applied potential values. Besides, the RR values for all cases are greater than one, meaning that negative current values are always greater in magnitude than positive current values. As explained earlier, in cases of ($C_U/C_L \geq 0.5$), the currents recorded for negative applied potentials are higher thatn the currents recorded for positive applied potentials. In contrast, for low concentration ratio values ($C_U/C_L < 0.5$) the RR are less than one, meaning that the magnitude of the negative ionic current is lower than that of the positive ionic current.

4.2. Numerical results

The coupled system of PNP-NS equations must be solved simultaneously for the given geometry using appropriate boundary conditions. Given the complexity of asymmetric domain, an analytical solution of this system of equations will not be possible. The nonlinear system of equations was solved numerically with the commercial finite-element package COMSOL Multiphysics 5.3a, which is suitable for irregular geometries. The computational domain is discretized into quadratic triangular elements of various sizes. Due to the formation of an EDL near the charged nanochannel wall,

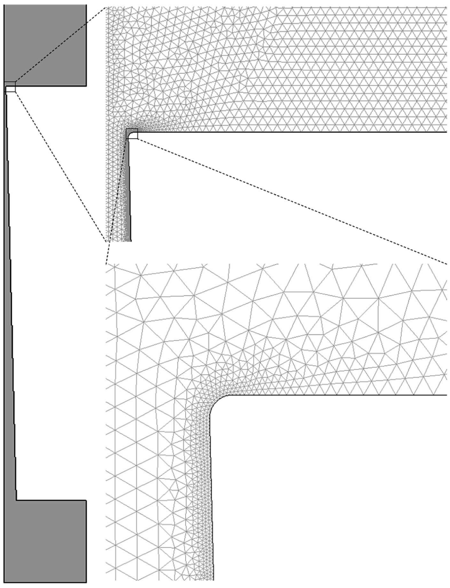

Figure 7. The computational domain with the mesh used in the FEM.

finer mesh was used near the channel wall to achieve better quality for simulations. The total number of elements is approximately 4×10^5, which is 25% more than similar numerical computations, and the average mesh size is about 11.7 nm. Moreover, in the regions close to the tip of the nanochannel in which EDLs may overlap, a finer mesh was used. The computational domain with the mesh used in the FEM is shown in Figure 7. The accuracy of the numerical method has been investigated by simulating some benchmark problems involving EDLs with theoretical solutions (e.g. electrical potential distribution near a charged surface, electroosmotic flow in a straight nanochannel), which has been previously confirmed by other researchers [16,27]. The convergence and grid independence of the obtained solutions were investigated by systematic grid refinement tests. For the simulations, the computational domain was assumed to be in an aqueous solution of KCl at room temperature, using the following parameters: $T = 300$ K, $D(\mathrm{K}^+)=1.95\times10^{-9}$ m^2/s, $D(\mathrm{Cl}^-)=2.03\times10^{-9}$ m^2/s, $\varepsilon=7.08\times10^{-10}$ F/m, $\mu=1\times10^{-3}$ Pa·s, and $\rho=1\times10^3$ kg/m^3. The numerical solution produces the concentration distribution $c_i(r)$ for the two species, the potential distribution $\varphi(r)$, velocity $u(r)$, and pressure $p(r)$ distribution in the domain. Analysis of these quantities helps to understand the possible mechanisms of the ICR phenomenon.

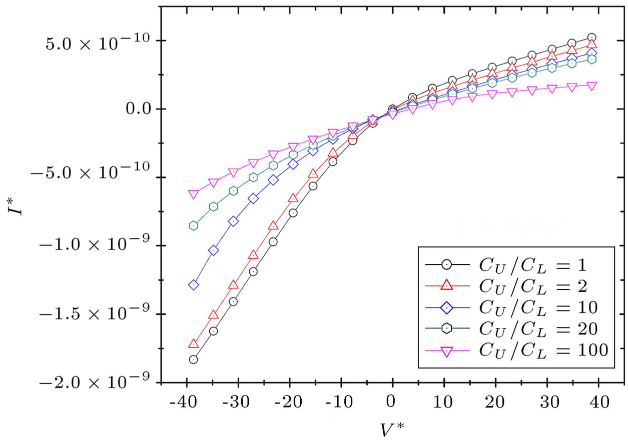

Figure 8. Numerical results of ionic current variation with applied voltage across various electrolyte gradients ($C_u/C_l \geq 1$).

Typical numerical results of the ionic mass transport in an asymmetric nanochannel simultaneously exposed to an axial electric field and a KCl concentration gradient are presented. Figure 8 shows the current-voltage (I-V) characteristics of a single asymmetric nanochannel under different electrolyte concentration gradients. Current responses to the applied bias voltage were calculated from -1 V to $+1$ V in increments of 100 mV. Five KCl solutions of 1, 5, 10, 50 and 100 mM were examined for comparison with the experimental results obtained. Similar to the experimental study, the upper fluid well was fixed at 100 mM KCl, while the concentrations of the lower fluid well were varied for the first set of numerical study. The current rectification is clearly visible in the reference case. The magnitude of the current recorded for -1 V is approximately three times higher than the magnitude of the current recorded for $+1$ V. As seen in the Figure 8, the character of the current-voltage (I-V) curves strongly depends on the bulk concentration of the KCl electrolyte solution. As defined in the experimental study, positive ionic current was defined as a current directed from the large opening (base) to the small opening (tip) when a positive voltage ($V = \varphi_{base} - \varphi_{tip} > 0$) is applied. As can be seen from Figure 8, the magnitude of a negative ionic current under a negative voltage is higher than under a positive voltage. As a result, the preferential direction of ionic current is still tip to base.

In the second set, the lower fluid well was fixed with 100 mM KCl, while the concentrations of the upper fluid well were variably changed this time. The results can be seen in Figure 9. An important phenomenon can be seen here when analyzing the $C_U/C_L = 0.5$ case. Compared to the same case in Figure 8, negative current values were still increasing, but at a slower rate, meaning the rectification was trying to reverse itself. As mentioned earlier, the preferred ionic current direction is tip to base, so current values are higher for negative potentials. On the other hand, the ionic current also tends to be higher for the reverse direction (base to tip), which is a direct consequence of the reversed concentration gradient. It is clear that these two properties compete each other, and as shown in the figure, the preferred direction dominates the effect of the inverted concentration gradient here. As

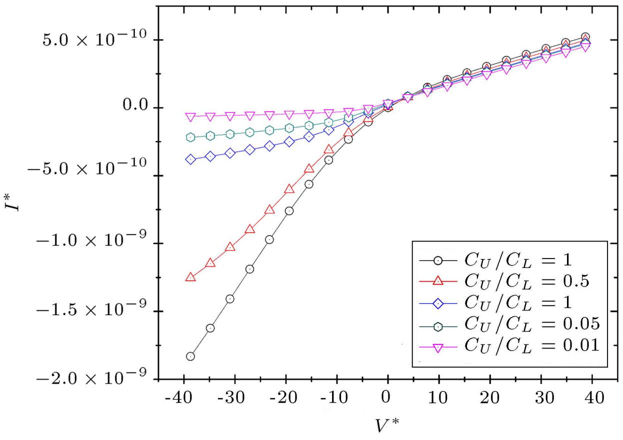

Figure 9. Numerical results of ionic current variation with applied voltage across various electrolyte gradients ($C_u/C_l \leq 1$).

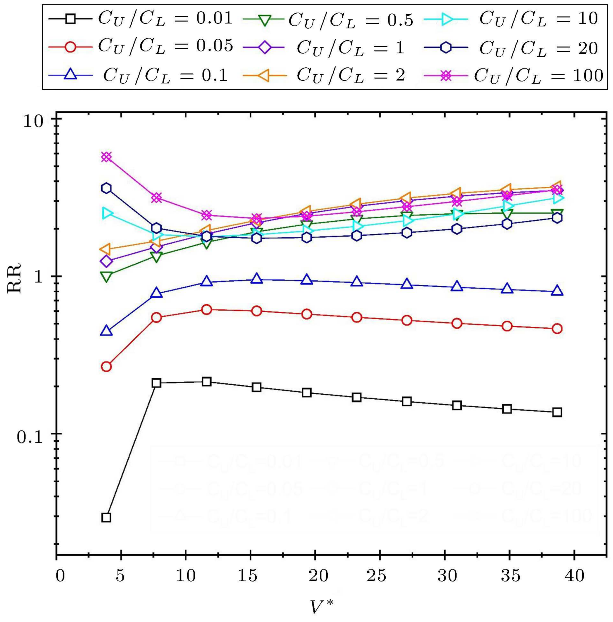

Figure 10. Current rectification ratio as a function of the applied potential difference across the nanochannel cosrresponding to the numerical results in Figures 8 and 9.

a result, negative ionic current values are still higher and rectification is not reversed in this case. For higher concentration gradients ($C_U/C_L < 0.5$), the preferential direction is dominated by the effect of the inverted concentration gradients and existing rectifications are reversed. The most important physical result here is that the concentration gradient applied between the tip and the base of the asymmetric nanochannel can not only rectify the ion current, but also reverse the direction of the rectification.

Figure 10 shows the RR values as a function of the magnitude of the applied bias voltage under the same conditions as Figures 8 and 9. In the case of the highest concentration ratio $C_U/C_L = 100$, the highest RR value is obtained for lowest applied potential. Conversely, in the case of the lowest concentration ratio $C_U/C_L = 1$, the lowest RR value is obtained for the same applied potential. In addition, all RR values for all cases are greater than one, that is, the magnitudes of the negative current values are always greater than the magnitudes of the positive current values.

An interesting observation about this example (Figure 10) is that for lower concentration ratio values (C_U/C_L=1 and 2), the RR increases with applied voltage, while for higher concentration ratios (C_U/C_L=10, 20, and 100) it first decreases and then slowly increases again. The physics underlying these results can be explained by examining some of the current-voltage values obtained for low applied potentials. For instance, the magnitude of the ionic current value is 2.87 when $V^* = 3.87$ and C_U/C_L=1. However, the magnitude of the ionic current value is 1.58 when $V^* = 0$ and C_U/C_L=100. This reveals that, although no electric potential is applied, an ionic current is generated by an amount comparable to the case where the potential of 3.87 is applied. As a result, it was concluded that high concentration gradients have as much effect on ionic current as low applied potentials. Moreover, because the concentration of the upper fluid well is higher, the ionic current direction is from the upper fluid well to the lower one, which means a negative current. When a negative potential (−3.87) is applied between the fluid wells, it increases the ionic current since it is in the same direction as the existing ionic current. On the other hand, the applied positive potential is in the opposite direction and stops the existing ionic current and causes a sharp decrease. As a result, the ionic current differences between the corresponding low negative and positive potential values are very high. Therefore, the highest rectification values are direct consequences of this physical fact.

As previously explained in Figure 9, the currents recorded for applied potential are higher than the currents recorded for +1 V applied potential when $C_U/C_L = 1$ and 0.5. In contrast, they are lower than the current values recorded for +1 V applied potential when $C_U/C_L = 0.1$, 0.05, and 0.01 due to the reversal of the rectification direction. This fact can also be seen in the corresponding RR curves (Figure 10). For low concentration ratio values (0.1, 0.05, 0.01), the RR are loess than 1, meaning that the recorded magnitudes of negative ionic current values are smaller than the recorded magnitudes of positive ionic current values.

In order to make a clearer comparison of the experimental and numerical results, the ionic current graphs corresponding to the applied potentials for each applied concentration gradient case are compared one by one as in Figure 11. To make this comparison, the numerical results obtained as nondimensional were converted back to the dimensional form. As can be

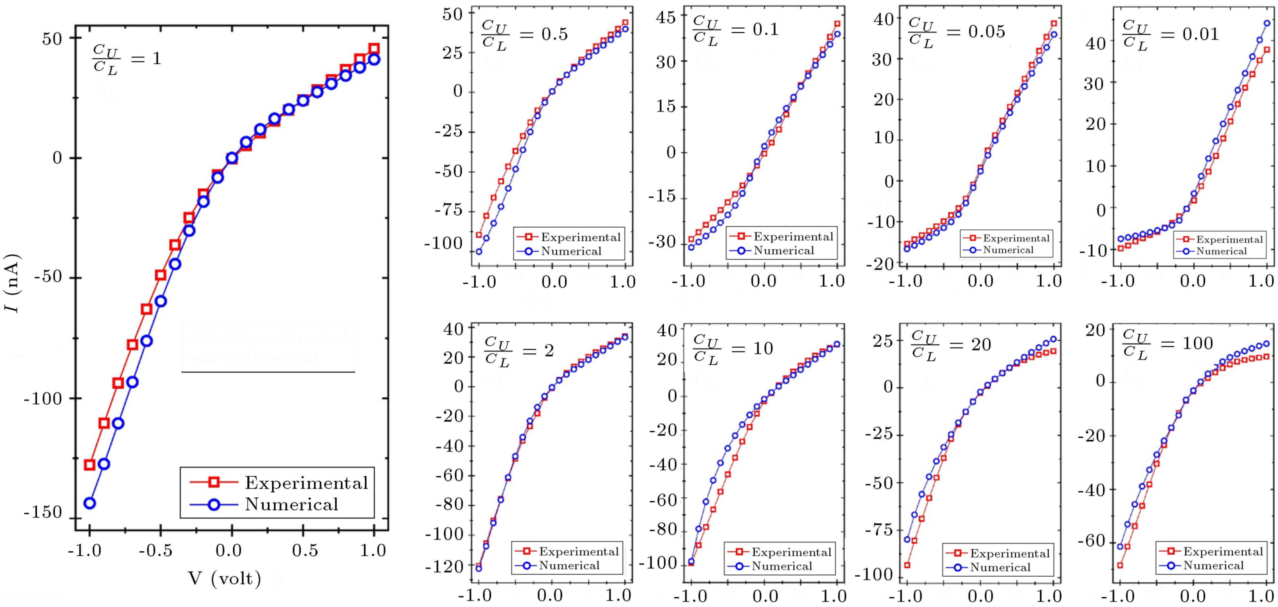

Figure 11. Comparison of experimental and numerically obtained I-V curves.

seen from all the graphs in Figure 11, the experimental and numerical results are quite congruent in all cases. The I-V curves have similar trends and there are significant divergences in only certain applied potential values. Again, in all cases, ionic rectification is clearly visible. When all obtained data points are compared, the Mean Absolute Error (MAE) between the experimental and numerical I-V curves is 3.71 nA, while the maximum and minimum errors are 17.26 nA and 0.01 nA, respectively.

It is necessary to examine the potential and concentration distribution profiles along the asymmetric nanochannel to identify possible mechanisms for ICR. Figure 12 shows the distributions of electric potential along the axis of the nanochannel with a surface charge of -0.01 C/m^2 for applied biases of V^*=+ 38.7 (P) and V^*=$-$38.7 (N). Profiles were obtained for the following three different cases: C_U/C_L=100 (I), C_U/C_L=1 (II), and C_U/C_L=0.01 (III). The nanochannel base is located at z^*=40 and the tip is located at z^*=240. When an external bias is applied across the asymmetric nanochannel, most of the potential drop occurs near the tip of the nanochannel where the resistance is greatest. This is observed across both positive and negative biases in the figure. The potential variations within the fluid wells $z^* < 40$ and $z^* > 240$ are very small. In case IIIN, the potential is almost the same in the region of $0 < z^* < 238$, but drops abruptly near the negatively charged tip where the resistance is greatest. This happens in case IIIN because the concentration of the lower fluid well is much higher than the concentration of the upper fluid well, and the applied electric field is from tip to base (negative applied potential). Most of the negative ions move from the lower fluid well to the upper one without remarkable disturbance until they are near the tip. The negatively charged nanochannel tip repels negative ions. As mentioned above, the potential drops abruptly as the resistance of the channel is greatest at the tip of the asymmetric nanochannel.

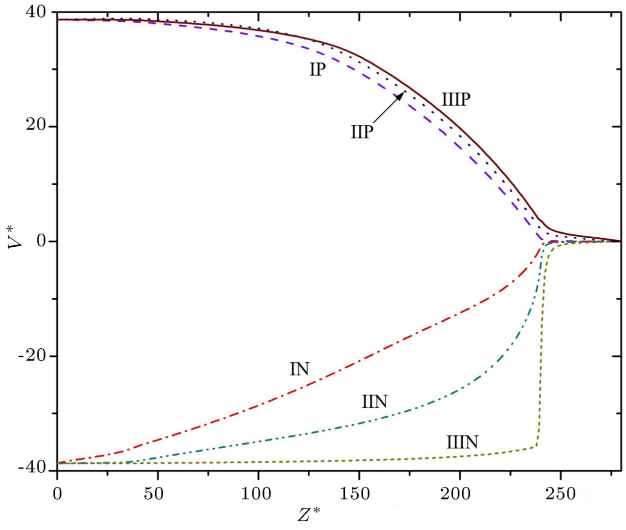

Figure 12. Variation of the electric potential along the axis of the nanochannel for applied biases of $V^* = +38.7$ (P) and $V^* = -38.7$ (N). The Roman numbers I, II and III correspond to $C_U/C_L = 100$, $C_U/C_L = 1$, and $C_U/C_L = 0.01$ respectively.

To better understand the ICR in a asymmetric nanochannel, cross sectional average ionic concentrations of cations (a) and anions (b) were investigated near the tip of the nanochannel for cases of C_U/C_L = 100 (I), 1 (II), and 0.01 (III) when V^*=+ 38.7 (top row)

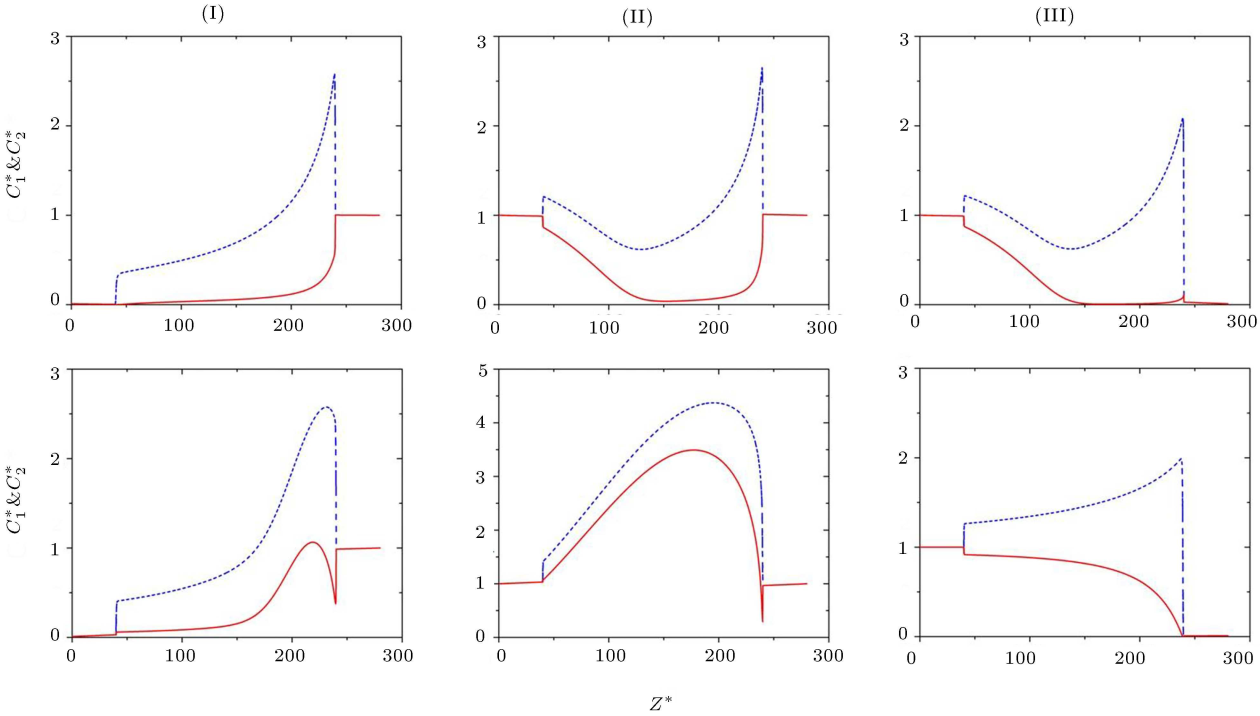

Figure 13. Cross-sectional averaged ionic concentrations (dashed line for K^+, and solid line for Cl^-) along the nanochannel. The Roman numbers I, II, and III correspond to $C_U/C_L = 100$, $C_U/C_L = 1$, and $C_U/C_L = 0.01$ respectively.

and V^*=−38.7 (bottom row) as shown in Figure 13. When a negative bias is applied, the positive ions migrate in the positive axial direction. Some positive ions migrate from the tip attached upper fluid well into the nanochannel, resulting in depletion of positive ions in the upper fluid well and enrichment of positive ions near the tip of the nanochannel. In contrast, some negative ions are drawn into the nanochannel from the lower fluid well, which is well connected to the base, and migrate to the tip in the negative axial direction. Far from the tip of the nanochannel, where the radius is greater than the thickness of the EDL, the Cl^{-1} ions are repelled from the negatively charged wall, resulting in a higher concentration in the core of the nanochannel and a lower concentration near the wall. Near the tip of the nanochannel, where the effect of the EDL is dominant, the concentration of negative ions is lower than the bulk concentration. Moreover, since the wall of the nanochannel is negatively charged, it also repels Cl^{-1} ions from the nanochannel tip. This combination gives rise to the formation of a region in the upper fluid well (near the tip) where the concentration of Cl^{-1} ions is above the bulk concentration. Near the negatively charged wall, the concentration of Cl^{-1} ions is reduced primarily due to the effect of EDL in the vicinity of the negatively charged wall. As clearly seen in the Figure 13, the amount of cation (K^+) in the nanochannel is always greater than the amount of anion (Cl^{-1}). In addition, a detailed calculation of the ion ratio [number of K^+/number of Cl^{-1}] in the $z^* = 239$ region located just inside the tip of the channel was made for each of these cases and an average value of 43.06 was found for this region.

The spatial distributions of ions near the vicinity of the tip helps us better understand ICR in an asymmetric nanochannel. The spatial distributions of the dimensionless concentrations of the cations (K^+) and anions (Cl^{-1}) are studied near the tip of the nanochannel for $C_U/C_L = 100$ (I), 1 (II), and 0.01 (III) when $V = +1$ V (Figure 14) and $V = -1$ V (Figure 15). When a positive potential is applied, negative ions move from the upper fluid well to the lower fluid well. However, a significant amount of negative ions are repelled from the negatively charged nanochannel, leading to higher concentration in the middle, and a lower concentration near the wall. In contrast, positive ions move from the lower fluid well toward the upper one. Due to the electrostatic interaction, the nanochannel wall attracts a significant amount of positive ions. When a negative potential is applied, positive ions move along the nanochannel from the upper fluid well to the lower one. This movement maintains the increase of positive ions in the upper fluid well and the decrease in the nanochannel, particularly near the tip. In turn, negative ions start to move from the lower fluid well to the upper fluid well. Inside the channel, the region away from the tip where the radius is relatively wider, the negatively charged nanochannel wall repels anions, resulting in higher anion concentration in the middle of the nanochannel

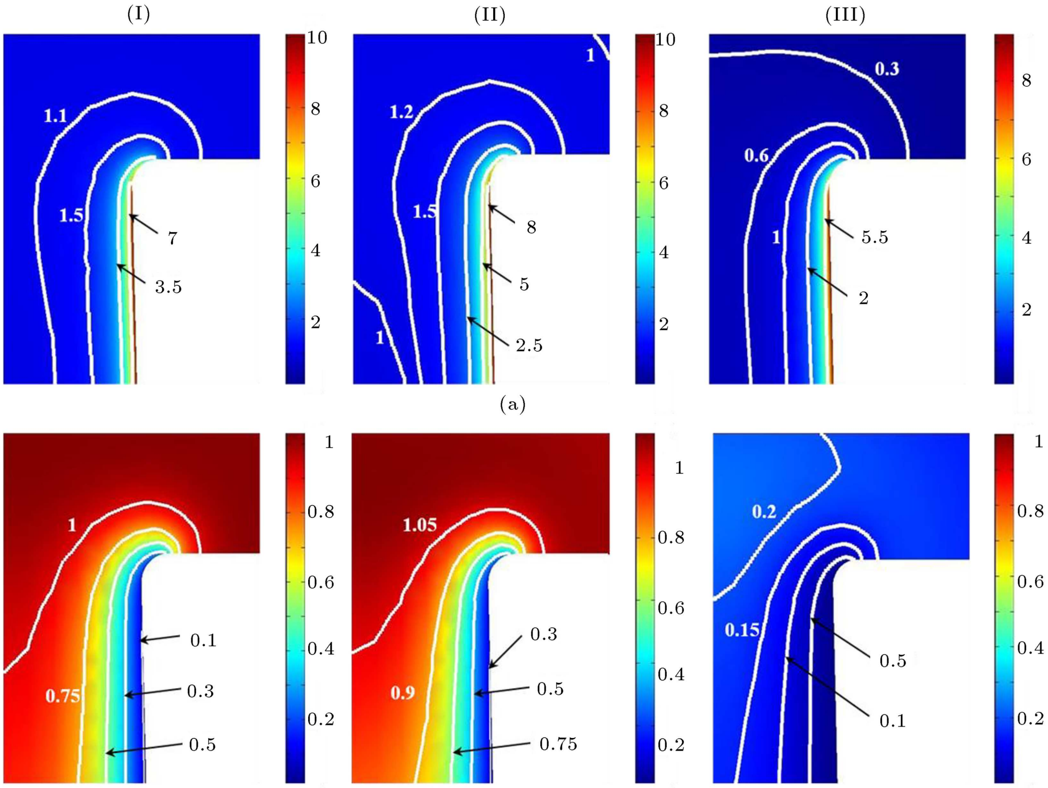

(a)

(b)

Figure 14. Distribution of the dimensionless concentration of positive (a) and negative (b) ions near the tip of the nanochannel for $C_U/C_L = 100$ (I) , 1 (II), and 0.1 (III) at $V^* = +38.7$.

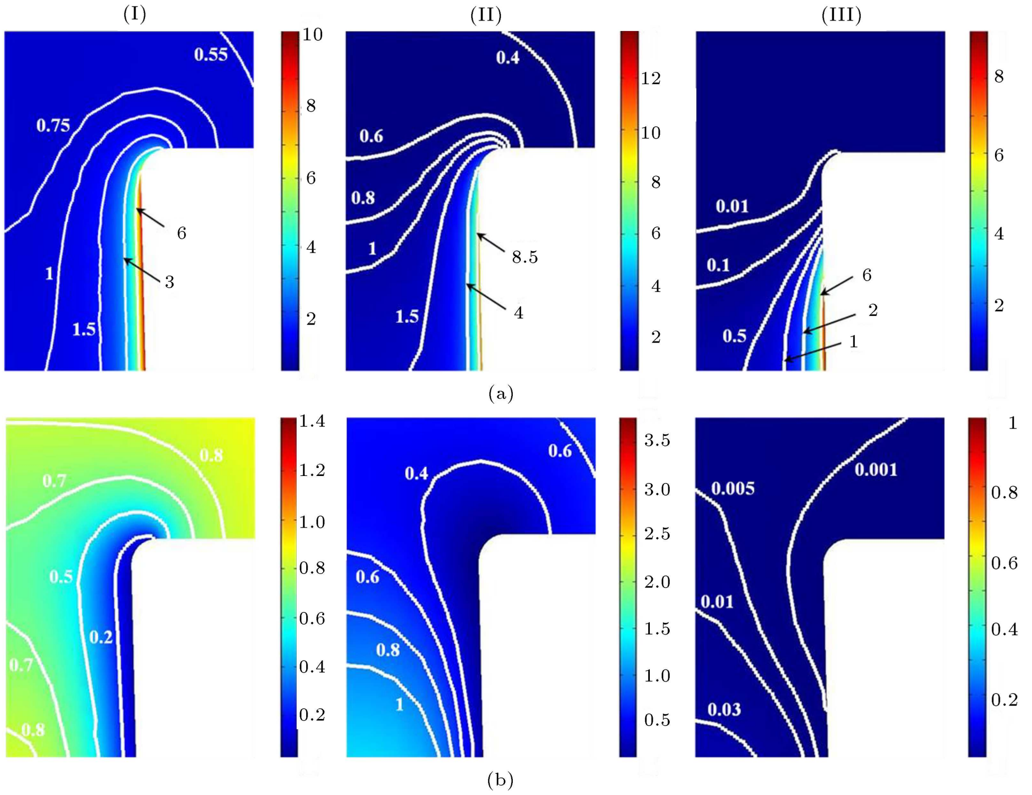

(a)

(b)

Figure 15. Distribution of the dimensionless concentration of positive (a) and negative (b) ions near the tip of the nanochannel for $C_U/C_L = 100$ (I), 1 (II), and 0.1 (III) at $V^* = -38.7$.

and lower concentration near the nanochannel wall. Because the effect of EDL dominates near tip, the concentration of negative ions is lower than the bulk concentration.

5. Conclusion

Ionic Current Rectification (ICR) in asymmetrical nanochannels subjected to axial electric field and concentration gradient was investigated experimentally and numerically. The ICR phenomenon in asymmetric nanochannels was extensively studied using a continuum model consisting of Nernst-Planck equations for ionic concentrations, Poisson's equation for electric potential, and Navier-Stokes equations for flow field. To validate the numerical results, experimental studies were performed using a membrane containing an asymmetric nanochannel immersed in a KCl solution. An experimental setup different from the literature and a nanochannel made of Thermoplastic Polyurethane (TPU) was used, which has not been used before in similar studies. Various concentration gradients were imposed between the two apertures of the nanochannel and the ICR phenomenon was investigated by applying two different electrical polarities on the experimental setup.

Some interesting properties of asymmetric nanochannels such as ion selectivity, voltage-dependent solution conductivity and ion current rectification have been observed experimeentally. The measured I-V curves showed that there is a preferential current direction for ion transport in response to the different applied bias polarities. The primary reason for the preferred current direction is that inner surface of the nanochannel in contact with the electrolyte forms an Electric Double Layers (EDL). The negatively charged TPU polymer surface attracted positive charges, creating an EDL of significant thickness, which played an important role in the ion transport along the nanochannel. Therefore, at the tip of the asymmetric nanochannel where the channel walls are relatively close to each other, these formed EDLs overlap and creates a gating mechanism. As a result of this, the nanochannel acts as ion selective, just like a filter. The important finding here is that the thick EDL formed due to the surface feature of the TPU reveals the current rectification phenomenon, which is evident in nanochannels under 100 nm radius, also in a nanochannel with 300 nm radius. Moreover, the superimposed electrolyte concentration gradient affects the ionic current flowing through the nanochannel. The degree and direction of the ICR depend on the magnitude and direction of the electrolyte gradient applied along nanochannel, therefore, the ICR can be tuned by adjusting the electrolyte concentrations in the two fluid wells connecting the nanochannel.

The verified continuum model consisting of coupled Poisson-Nernst-Planck equations and Navier-Stokes equations is applied to study ICR in an asymmetric nanochannel. The predicted diode-like I-V curves are in qualitative agreement with the experiments. In the absence of an electrolyte gradient, typically, the preferential current direction of a negatively charged nanochannel is oriented tip to base due to the ion depletion under negative voltage and ion enrichment under positive voltage. However, the preferential current direction reverses when a sufficient electrolyte gradient directed from the base to the tip is imposed. The ICR originates from the surface charge of the nanochannel, which generates an asymmetric ion distribution along the asymmetric nanochannel, rendering the asymmetric nanochannel similar to a nanofluidic diode.

Controlling ionic transport through a nanochannel is one of the most important issues of nanofluidics studies. Through this study, it was shown that a concentration gradient applied along the axis of the nanochannel affects the distributions of electric potential and ionic concentrations within the nanochannel, resulting in a difference in I-V responses. Therefore, it has been shown that the degree and direction of the ICR can be controlled by adjusting the electrolyte concentrations in the two fluid wells. Moreover, it has been shown that nanochannels with large radii also cause current rectification when electrolyte is used at a concentration that will ensure the formation of EDL of sufficient thickness on the nanochannel surface.

Acknowledgements

The experimental studies were performed at the Institute of Micro/Nano Technology of Old Dominion University, Norfolk, VA, USA.

Conflict of interest statement

Authors declare that there is no conflict of interest.

Author contributions

M. Bakirci conceived of the presented idea, carried out the experiments, performed the numerical simulations, took the lead in writing the manuscript. R. Garren aided in interpreting the results and worked on the manuscript. All authors discussed the results and contributed to the final manuscript as well as they approve this final version of the manuscript.

References

1. Spitzberg, J.D., Zrehen, A., van Kooten, X.F., et

al. "Plasmonic-nanopore biosensors for superior single-molecule detection", *Adv. Mater.*, **31**(1900422), pp. 1–18 (2019). DOI: 10.1002/adma.201900422

2. Cui, F., Yue, Y., Zhang, Y., et al. "Advancing biosensors with machine learning", *ACS Sens.*, **5**(11), pp. 3346–3364 (2020). DOI: 10.1021/acssensors.0c01424
3. Haleem, A., Javaid, M., Singh, R.P., et al. "Biosensors applications in medical field: a brief review", *Sens. Intern.*, **2**(100100), pp. 1–10 (2021). DOI: 10.1016/j.sintl.2021.100100
4. Zhao, J., He, G., Huang, S., et al. "Etching gas-sieving nanopores in single-layer graphene with an angstrom precision for high-performance gas mixture separation", *Sci. Adv.*, **5**(1), pp. 1–9 (2019). DOI: 10.1126/sciadv.aav1851
5. Wang, S., Yang, L., He, G., et al. "Two-dimensional nanochannel membranes for molecular and ionic separations", *Chem. Soc. Rev.*, **49**, pp. 1071–1089 (2020). DOI: 10.1039/C9CS00751B
6. Shen, Y.J., Kong, Q.R., Fang, L.F., et al. "Construction of covalently-bonded tannic acid/polyhedral oligomeric silsesquioxanes nanochannel layer for antibiotics/salt separation", *J. Membr. Sci.*, **623**, pp. 1–8 (2021). DOI: 10.1016/j.memsci.2020.119044
7. Shankla, M. and Aksimentiev, A. "Step-defect guided delivery of DNA to a graphene nanopore", *Nature Nanotech.*, **14**, pp. 858–865 (2019). DOI: 10.1038/s41565-019-0514-y
8. Shi, X., Verschueren, D.V., and Dekker, C. "Active delivery of single DNA molecules into a plasmonic nanopore for label-free optical sensing", *Nano Lett.*, **18**(12), pp. 8003–8010 (2018). DOI: 10.1021/acs.nanolett.8b04146
9. Seifollahi, Z. and Ashrafizadeh S.N. "Effect of charge density distribution of polyelectrolyte layer on electroosmotic flow and ion selectivity in a conical soft nanochannel", *Chem. Eng. Sci.*, **261**, pp. 1–13 (2022). DOI: 10.1016/j.ces.2022.117986
10. Chen, R., Balla, R.J., Lima, A., et al. "Characterization of nanopipet-supported ITIES tips for scanning electrochemical microscopy of single sloid-state nanopores", *Anal. Chem.*, **89**(18), pp. 9946–9952 (2017). DOI: 10.1021/acs.analchem.7b02269
11. Zhou, P. and Su, B. "Enhanced electrochemiluminescence at silica nanochannel membrane studied by scanning electrochemical microscopy", *J. Electranaly. Chem.*, **904**, pp. 1–6 (2022). DOI: 10.1016/j.jelechem.2021.115943
12. Bucci, G. and Spakowitz, A.J. "Systematic approach toward accurate and efficient DNA sequencing via nanoconfinement", *ACS Macro Lett.*, **9**(8), pp. 1184–1191 (2020). DOI: 10.1021/acsmacrolett.0c00423
13. Yong, H., Molcrette, B., Sperling, M., et al. "Regulating translocation of DNA through poly(n-isopropylacrylamide)-decorated switchable nanopores by cononsolvency effect", *Macromolec.*, **54**(9), pp. 4432–4442 (2021). DOI: 10.1021/acs.macromol.1c00215
14. Zhang, X., Zhang, L. and Li, J. "Peptide-modified nanochannel system for carboxypeptidase B activity detection", *Analyt. Chim. Acta.*, **1057**, pp. 36–43 (2019). DOI: 10.1016/j.aca.2019.01.018
15. Wu, X., Che, C., Wang, X., et al. "Ionic signal enhancement by space charge effect through the DNA rolling circle amplification on the outer surface of nanochannels", *Anal. Chem.*, **93**(48), pp. 16043–16050 (2021). DOI: 10.1021/acs.analchem.1c03631
16. Devarakonda, S., Kim, S., Ganapathysubramanian, B., et al. "Designing asymmetrically modified nanochannel sensors using virtual EIS", *Electrochim. Acta.*, **403**, pp. 1–10 (2022). DOI: 10.1016/j.electacta.2021.139694
17. Gupta, A., Zuk, P.J., and Stone, H.A. "Charging dynamics of overlapping double layers in a cylindrical nanopore", *Phy. Rev. Lett.*, **125**, p. 076001 (2020). DOI: 10.1103/PhysRevLett.125.076001
18. Li, C., Liu, Z., Qiao, N., et al. "The electroviscous effect in nanochannels with overlapping electric double layers considering the height size effect on surface charge", *Electrochim. Acta.*, **419**, pp. 1–9 (2022). DOI: 10.1016/j.electacta.2022.140421
19. Ramirez, P., Manzanares, J.A., Cervera, J., et al. "Nanopore charge inversion and current-voltage curves in mixtures of asymmetric electrolytes", *J. of Memb. Sci.*, **563**, pp. 633–642 (2018). DOI: 10.1016/j.memsci.2018.06.032
20. Davis, S.J., Macha, M., Chernev, A., et al. "Pressure-induced enlargement and ionic current rectification in symmetric nanopores", *Nano Lett.*, **20**(11), pp. 8089–8095 (2020). DOI: 10.1021/acs.nanolett.0c03083
21. Ma, L., Li, Z., Yuan, Z., et al. "Modulation of ionic current rectification in ultrashort conical nanopores", *Anal. Chem.*, **92**(24), pp. 16188–16196 (2020). DOI: 10.1021/acs.analchem.0c03989
22. Xioang, T., Zhang, K., Jiang, Y., et al. "Ion current rectification: from nanoscale to microscale", *Sci. China Chem.*, **62**, pp. 1346–1359 (2019). DOI: 10.1007/s11426-019-9526-4
23. Liu, J., Fu, B., and Zhang, Z. "Ionic current rectification triggered photoelectrochemical chiral sensing platform for recognition of amino acid enantiomers on self-standing nanochannel arrays", *Anal. Chem.*, **92**(13), pp. 8670–8674 (2020). DOI: 10.1021/acs.analchem.0c02341
24. Zhang, S., Chen, W., Song, L., et al. "Recent advances in ionic current rectification based nanopore sensing: a mini-review", *Sens. Actu. Reports.*, **3**, pp. 1–7 (2021). DOI: 10.1016/j.snr.2021.100042
25. Poggioli, A.R., Siria, A., and Bocquet, L. "Beyond the tradeoff: dynamic selectivity in ionic transport and current rectification", *J. Phys. Chem. B.*, **123**(5), pp. 1171–1185 (2019). DOI: 10.1021/acs.jpcb.8b11202
26. Rabinowitz, J., Edwards, M.A., Whitter, E., et al. "Nanoscale fluid vortices and nonlinear electroosmotic flow drive ion current rectification in the presence of concentration gradients", *J. Phys. Chem. A.*, **123**(38), pp. 8285–8293 (2019). DOI: 10.1021/acs.jpca.9b04075

27. Zhou, Y., Liao, X., Han, J., et al. "Ionic current rectification in asymmetric nanofluidic devices", *Chinese Chem. Lett.*, **31**(9), pp. 1–9 (2020). DOI: 10.1016/j.cclet.2020.05.033

28. Ma, L., Li, Z., Yuan, Z., et al. "Modulation of ionic current rectification in ultrashort conical nanopores", *Anal. Chem.*, **92**(24), pp. 16188–16196 (2020). DOI: 10.1021/acs.analchem.0c03989

29. Li, Z.Q., Wang, Y., Wu, Z.Q., et al. "Bioinspired multivalent ion responsive nanopore with ultrahigh ion current rectification", *J. Phys., Chem. C.*, **123**(22), pp. 13687–13692 (2019). DOI: 10.1021/acs.jpcc.9b02279

30. Dartoomi, H., Khatibi, M., and Ashrafizadeh, S.N. "Enhanced ionic current rectification through innovative integration of polyelectrolyte bilayers and charged-wall smart nanochannels", *Anal. Chem.*, **95**(2), pp. 1522–1531 (2022). DOI: 10.1021/acs.analchem.2c04559

31. Cai, J., He, Q., Song, L., et al. "Ion current rectification behavior of conical nanopores filled with spatially distributed fixed charges", *J. Phys. Chem. C.*, **123**(43), pp. 26299–26308 (2019). DOI: 10.1021/acs.jpcc.9b06872

32. Davis, S.J., Macha, M., Chernev, A., et al. "Pressure-induced enlargement and ionic current rectification in symmetric nanopores", *Nano Lett.*, **20**(11), pp. 8089–8095 (2020). DOI: 10.1021/acs.nanolett.0c03083

33. Kim, Y.D., Choi, S., Kim, A., et al. "Ionic current rectification of porous anodic aluminum oxide (AAO) with a barrier oxide layer", *ACS Nano.*, **14**(10), pp. 13727–13738 (2020). DOI: 10.1021/acsnano.0c05954

34. Wen, C., Zeng, S., Li, S., et al. "On rectification of ionic current in nanopores", *Anal. Chem.*, **91**(22), pp. 14597–14604 (2019). DOI: 10.1021/acs.analchem.9b03685

35. Zhao, C., Zhang, H., Hou, J., et al. "Effect of anion species on ionic current rectification properties of positively charged nanochannels", *ACS Appl. Mater. Interfaces.*, **12**(25), pp. 28915–28922 (2020). DOI: 10.1021/acsami.0c08263

36. Atiqah, A., Jawaid, M., Sapuan, S.M., et al. "Physical and thermal properties of treated sugar palm/glass fibre reinforced thermoplastic polyurethane hybrid composites", *J. of Mater. Res. and Tech.*, **8**(5), pp. 3726–3732 (2019). DOI: 10.1016/j.jmrt.2019.06.032

37. Ke, K., Bonab, S., Yuan, D., et al. "Piezoresistive thermoplastic polyurethane nanocomposites with carbon nanostructures", *Carbon.*, **139**, pp. 52–58 (2018). DOI: 10.1016/j.carbon.2018.06.037

38. Liu, C., Wu, W., Shi, Y., et al. "Creating Mxene/reduced graphene oxide hybrid towards highly fire safe thermoplastic polyurethane nanocomposites", *Compo. Part B: Eng.*, **203**, 108486 (2020). DOI: 10.1016/j.compositesb.2020.108486

39. Nelson, M.D., Ramkumar, N., and Gale, B.K. "Flexible, transparent, sub-100 μm microfluidic channels with fused deposition modeling 3d-printed thermoplastic polyurethane", *J. of Micromech. and Microeng.*, **29**(9), 095010 (2019). DOI: 10.1088/1361-6439/ab2f26

40. Jaso, V., Cvetinov, M., Rakic, S., et al. "Bio-plastics and elastomers from polylactic acid/thermoplastic polyurethane blends", *J. of Appl. Poly. Sci.*, **131**(22), p. 41104 (2014). DOI: 10.1002/app.41104

41. Jing, X., Mi, H.Y., Huang, H.X., et al. "Shape memory thermoplastic polyurethane (TPU)/poly(epsilon-caprolactone) (PCL) blends as self-knotting sutures", *J. of Mech. Behav. of Biomed. Mater.*, **64**, pp. 94–103 (2016). DOI: 10.1016/j.jmbbm.2016.07.023

42. Zheng, Y., Dong, R., Shen, J., et al. "Tunable shape memory performances via multilayer assembly of thermoplastic polyurethane and polycaprolactone", *ACS Appl. Mater. Interf.*, **8**(2), pp. 1371–1380 (2016). DOI: 10.1021/acsami.5b10246

43. Guo, Y., Yan, L., Zeng, Z., et al. "TPU/PLA nanocomposites with improved mechanical and shape memory properties fabricated via phase morphology control and incorporation of multi-walled carbon nanotubes nanofillers", *Poly. Eng. and Sci.*, **60**, pp. 1118–1128 (2020). DOI: 10.1002/pen.25365

44. Yu, F. and Huang, H.X. "Simultaneously toughening and reinforcing poly(lactic-acid)/thermoplastic polyurethane blend via enhancing interfacial adhesion by hydrophobic silica nanoparticles", *Poly. Test.*, **45**, pp. 107–113 (2015). DOI: 10.1016/j.polymertesting.2015.06.001

45. Jaso, V., Rodic, M.V., and Petrovic, Z.S. "Biocompatible fibers from thermoplastic polyurethane reinforced with polylactic acid microfibers", *Euro. Poly. J.*, **63**, pp. 20–28 (2015). DOI: 10.1016/j.eurpolymj.2014.11.041

46. Fan, Q., Qin, Z., Villmow, T., et al. "Vapor sensing properties of thermoplastic polyurethane multifilament covered with carbon nanotube networks", *Sen. and Act. B Chem.*, **156**(1), pp. 63–70 (2011). DOI: 10.1016/j.snb.2011.03.073

47. Yan, L., Xiong, T., Zhang, Z., et al. "Comparative study on TPU/multi-walled carbon nanotubes conductive nanocomposites for volatile organic compounds sensor applications", *J. of Poly. Res.*, **28**, p. 350 (2021). DOI: 10.1007/s10965-021-02717-5

48. Kim, K., Park, J., Suh, J., et al. "3D printing of multiaxial force sensors using carbon nanotube (CNT)/thermoplastic polyurethane (TPU) filaments", *Sen. and Act. A: Phy.*, **263**, pp. 493–500 (2017). DOI: 10.1016/j.sna.2017.07.020

49. Khatibi, M., Ashrafizadeh, S.N., and Sadeghi, A. "Covering the conical nanochannels with dense polyelectrolyte layers significantly improves the ionic current rectification", *Anal. Chim. Acta.*, **1122**, pp. 48–60 (2020). DOI: 10.1016/j.aca.2020.05.011

50. Sadeghi, A., Azari, M., and Hardt, S. "Electroosmotic flow in soft microchannels at high grafting densities", *Phy. Rev. Fluids.*, **4**(6), 063701 (2019). DOI: 10.1103/PhysRevFluids.4.063701

51. Schoch, R. B., van Lintel, H., and Renaud, P. "Effect of the surface charge on ion transport through nanoslits", *Phy. of Fluids.*, **17**, 100604 (2005). DOI: 10.1063/1.1896936

52. Pennathur, S. and Santiago, J.G. "Electrokinetic transport in nanochannels 2. Experimets", *Anal. Chem.*, **77**(21), pp. 6782–6789 (2007). DOI: 10.1021/ac0508346

Biographies

Murat Bakirci received his MS and PhD degrees from Old Dominion University, Norfolk, Virginia, USA. He was a ResearchAassistant at the Institute of Micro/Nano Technology of Old Dominion University. He also worked at Virginia Modeling Analysis and Simulation Center as a research assistant. Currently he holds a Lecturer position at the Faculty of Aeronautics and Astronautics at Tarsus University, Mersin, Turkey. His research interests include intelligent/unmanned systems, micro/nanofluidics, MEMS sensor applications, and dynamical system simulation.

Richard Garren is a PhD candidate at Batten College of Engineering and Technology, Old Dominion University, Norfolk, Virginia, USA. He received his BSc and MS degrees from Mechanical Engineering Department of Old Dominion University. His research interests include heat transfer, CFD, and micro/nanofluidics.